Sulfate reduction drives elevated methylmercury formation in water column of eutrophic freshwater lake

Benjamin D. Peterson[1,2,3,4*], Sarah E. Janssen[5], Brett A. Poulin[4], Jacob M. Ogorek[5], Amber White[2], Elizabeth A. McDaniel[3], Robert A. Marick[6], Grace J. Armstrong[2,5], Nicholas Scheel[7], Michael T. Tate[5], David P. Krabbenhoft[5], Katherine D. McMahon[2,3]

1. School of Freshwater Science, University of Wisconsin – Milwaukee, Milwaukee, WI 53204, United States
2. Environmental Chemistry and Technology Program, Department of Civil and Environmental Engineering, University of Wisconsin - Madison, Madison, Wisconsin 53706, United States
3. Department of Bacteriology, University of Wisconsin - Madison, Madison, WI 53706, United States
4. Department of Environmental Toxicology, University of California - Davis, Davis, CA 95616, United States
5. U.S. Geological Survey, Upper Midwest Water Science Center, Mercury Research Laboratory, Madison, Wisconsin 53726, United States
6. Department of Biochemistry, University of Wisconsin - Madison, Madison, Wisconsin 53706, United States
7. Freshwater and Marine Sciences, University of Wisconsin - Madison, Madison, Wisconsin 53706, United States

*Corresponding author: petersob@uwm.edu

Abstract

Mercury (Hg) contamination of aquatic food webs is controlled in part by the formation and accumulation of toxic and bioaccumulative methylmercury (MeHg). MeHg production is mediated by metabolically diverse microorganisms carrying the *hgcAB* gene pair, while the demethylation reaction is mediated by several biotic and abiotic processes. However, in the environment, the relative importance of these two processes on MeHg accumulation and the biogeochemical and microbial factors that influence them are still poorly characterized, especially in eutrophic environments. In this study, both Hg methylation and MeHg demethylation in a eutrophic urban freshwater lake were measured and linked to ambient MeHg concentrations and *hgcA* abundance and expression. High methylation rate potentials indicated *in situ* MeHg formation was a key source of MeHg to the water column and was driven by high *hgcA* abundance and transcription. Molybdate treatment decreased methylation rate potentials, highlighting the importance of sulfate reduction in driving MeHg formation in this system. Sulfate-reducing bacteria accounted for over 50% of the *hgcA* gene transcription, despite representing less than 10% of the *hgcA*-carrying microbial community. Across diverse genomes, an *arsR*-like transcriptional regulator preceded many *hgcA* sequences; these genes were transcriptionally active and were linked to lower relative *hgcA* expression. Overall, this study elucidates the microbial and biogeochemical processes that influence the *in situ* formation of MeHg in understudied eutrophic freshwater environments.

Introduction

Mercury (Hg) presents a persistent and severe global health risk due to contamination of important aquatic food sources.[1] Elemental gaseous Hg(0) is emitted by anthropogenic and natural sources into the atmosphere where it can be distributed regionally and globally before deposition to aquatic and terrestrial ecosystems. The conversion of inorganic Hg(II) to organic methylmercury (MeHg) leads to rapid bioaccumulation and biomagnification of Hg in aquatic and terrestrial foods webs.[2] This transformation is mediated by bacteria and archaea in hypoxic and anoxic environments.[3–5] In freshwater lacustrine environments, the importance of water column methylation as a source of MeHg to the aquatic food web is increasingly recognized.[6–11] Despite the global increase of lake eutrophication,[12] Hg methylation in eutrophic lakes remains highly understudied. Identifying how microbial and biogeochemical factors control MeHg formation will enable a mechanistic understanding of how water quality conditions influence this process; subsequently, this will inform efficient management and effective forecasting of local and global changes on the Hg contamination to aquatic food webs.

MeHg formation is regulated by two primary factors: the bioavailability of Hg(II) and the methylation capacity of the microbial community.[4,13] Hg(II) bioavailability is regulated by ligand chemistry; important factors include inorganic sulfide concentration and the concentration and composition of dissolved organic matter (DOM) (e.g., aromaticity, reduced sulfur content).[14–17] While the microbial capacity to methylate Hg(II) has been historically associated with sulfate-reducing bacteria (SRB),[5,18] the discovery of the Hg-methylating gene cluster *hgcAB* expanded the known diversity of putative Hg-methylating microbes.[3,19,20] When Hg(II) bioavailability is controlled for, *hgcA* abundance has been linked to measured microbial methylation capacity[13,21,22] and ambient MeHg concentrations[6] across different environments. Several

metagenomic studies have reported a low abundance or absence of *hgcA*-carrying (hgcA+) SRB in environments where sulfate-reduction is suspected or known to stimulate MeHg formation,[13,23,24] raising the possibility that other metabolic guilds influence methylation or that SRB play indirect roles in MeHg formation. One possible point of control is *hgcA* expression, which was originally hypothesized to be constitutive rather than actively regulated.[25] However, *hgcA* expression is controlled in some microorganisms by a transcriptional regulator homologous to *arsR*, a gene involved in arsenic cycling.[19,26] The evolutionary purpose and benefit of the *hgcAB* gene cluster is unknown, which limits an ecological understanding of its distribution.[20] Integrating microbial 'omics techniques and biogeochemical assay-based approaches is critical to advancing our understanding of the processes governing MeHg accumulation in the environment.

In this study, we investigated how water column MeHg concentrations within an urban eutrophic lake (Lake Mendota, Wisconsin, USA) were controlled by *in situ* Hg(II) methylation and MeHg demethylation under different redox conditions. We further sought to connect MeHg concentrations and production rates to microbial biogeochemical cycles and gene abundance/expression using water quality analyses, genome-resolved metagenomics, quantitative metatranscriptomics, and bacterial production assays. The role of SRB in MeHg formation and accumulation was specifically investigated using molybdate. Collectively, this study uses an interdisciplinary approach, including field experiments and 'omics methods, to advance our understanding of the microbial and biogeochemical drivers of MeHg accumulation in the water column of freshwater lakes.

Methods

Water and nucleic acid sample collection

Detailed information on site description can be found in the Supporting Information (SI) - Section S1.1. Briefly, samples were collected from the deepest basin (~24 m) in Lake Mendota in Madison, Wisconsin, USA (Fig. S1). Sampling occurred once during September and once during October in both 2020 and 2021. Temperature, dissolved oxygen (DO), and turbidity profiles were measured using a multiparameter sonde (YSI, Yellow Spring, OH). Samples were collected with a peristaltic pump and acid-washed C-flex tubing connected to Teflon tubing. Sulfide/sulfate samples were preserved in 1% zinc acetate. Iron and manganese samples were preserved in 1% nitric acid. Filter-passing metal samples were filtered using a 0.45 μm Acrodisc filter. Water for Hg analysis was collected with no headspace in a new 2 L polyethylene terephthalate glycol (PETG) bottle using clean hands/dirty hands technique, then filtered onto an ashed quartz fiber filter (QFF, nominal pore size 0.7 μm) at the USGS Mercury Research Laboratory (MRL) within 18 hours.[27] The filtrate was preserved to 1% hydrochloric acid (HCl) and the particulate samples were frozen until analysis. Dissolved gaseous mercury (DGM) was collected onto gold-coated bead traps in the field by purging 1L surface waters with high purity nitrogen gas.[28] Nucleic acid samples were collected by filtering approximately 200-700 mL of water onto a 0.2 μm Sterivex filter and preserved by flash-freezing with liquid nitrogen, followed by storage at -80˚C. For leucine uptake analysis in 2020, water was collected in-line into 3 mL syringes; in 2021, water was collected into N_2-flushed serum bottles, then transferred to syringes in the lab.

Hg methylation and demethylation incubations

Detailed incubation methods are in SI - Section S1.2. Three depths from the anoxic hypolimnion were selected on each sampling date (only two depths in October 2020) for incubations. Samples for Hg methylation incubations were collected into custom-designed, acid-washed, trilaminate bags with an ethylene vinyl alcohol Coex liner suitable for trace metal sampling and an oxygen-barrier layer (ProAmpac, Rochester, NY). At each incubation depth, ten bags were rinsed and filled with 450-550 mL of site water, eight with unfiltered water and two "control" bags with water filtered in-line using a 0.2 μm Sterivex filter (Millipore-Sigma). After collection, bags were resuspended in bins at the collection depth. Additional filtered water was collected in a bag at each depth to prepare the enriched stable isotope Hg standards. These bags were wrapped in foil, transported back to the lab, and stored in an anaerobic glovebox. Approximately five hours before the start of the incubations, enriched inorganic ^{198}Hg ($^{198}Hg(II)$), to track methylation, and enriched methyl-^{204}Hg ($Me^{204}Hg$), to track demethylation, were mixed with filtered water from each depth to create a "pre-equilibrated standard" with a final concentration of ~100 ng/L. After pre-equilibration, incubation bags were injected with the pre-equilibrated standard to an estimated final concentration of 0.75 ng/L of both $^{198}Hg(II)$ and $Me^{204}Hg$. Molybdate-inhibited bags were also injected with sodium molybdate to a final concentration equimolar to epilimnetic sulfate (~30.5 mg/L).[29,30] Samples were gently mixed and then the t_0 sample was immediately withdrawn from the bags and preserved to 1% HCl in a 125 mL PETG bottle. An unfiltered sample for sulfide analysis was also preserved to 1% zinc acetate. Incubation bags were then returned to their bins and resuspended in the lake at depth. Sample collection was repeated after approximately 24 hours (t_1) and either 80 or 48 hours in 2020 and 2021, respectively (t_2).

Geochemical analyses

All Hg analyses were conducted at the USGS MRL and passed required quality assurance and control metrics; complete details are in SI - Section S1.3. Ambient total Hg (THg) in filter-passing and particulate samples was analyzed by U.S. Environmental Protection Agency (EPA) Method 1631.[31] Briefly, THg was oxidized using bromine monochloride then quantified by cold vapor atomic fluorescence spectrometry (CVAFS) using a Brooks Rand TDM II and automated Merx-T, respectively (Brooks Rand Inc, Seattle, WA). Enriched isotope THg analysis was conducted by bromine monochloride oxidation, tin reduction, dual-stage gold amalgamation, and quantification by ICP-MS using a Merx-T (Brooks Rand Inc, Seattle, WA) coupled to an iCAP-RQ ICP-MS (Thermo-Fisher, Waltham, MA). DGM samples were analyzed via CVAFS.[28] Filter-passing and particulate ambient MeHg analyses and unfiltered enriched isotope assay samples were conducted using a modified version of U.S. EPA Method 1630 that included distillation, ethylation by sodium tetraethylborate, separation by gas chromatography, and quantification by isotope dilution using inductively coupled plasma mass spectrometry (ICP-MS) detection using a Merx-M (Brooks Rand Inc, Seattle, WA) coupled to an iCAP-RQ ICP-MS platform.[32–34] Ambient and isotope-enriched Hg speciation were calculated following previous methods.[35,36] Inorganic Hg(II) was calculated as follows:

Equation 1: $Hg(II) = THg - MeHg$.

The Hg(II) methylation rate potential (K_{met}; unit = day^{-1}) was calculated for each incubation using an integrated pseudo first-order rate law, assuming an irreversible reaction (for details, see SI - Section S1.4)[37,38]:

Equation 2: $K_{met} = -\ln(1 - ([Me^{198}Hg_{t2}] - [Me^{198}Hg_{t0}]) * [T^{198}Hg_{t0}]^{-1}) * t_2^{-1}$

153 Here, we define K_{met} as the Hg(II) methylation rate potential rather than a true rate since the
154 ^{198}Hg(II) in the pre-equilibrated standard may react differently than the ambient MeHg.[10,39] To
155 quantify the influence of SRB-inhibition on K_{met}, we describe the K_{met} values from the
156 molybdate-inhibited incubations as non-SRB-dependent K_{met} ($^{nonSRB}K_{met}$). We then calculated an
157 SRB-dependent K_{met} ($^{SRB}K_{met}$) for each sampling location as follows:

158 *Equation 3*: $$^{SRB}K_{met} = K_{met} - {}^{nonSRB}K_{met}$$

159 In *Equation 3*, K_{met} and $^{nonSRB}K_{met}$ represent the mean K_{met} and $^{nonSRB}K_{met}$ values, respectively, of
160 the four replicate incubations at the given sampling location.

161 Sulfide was analyzed spectrophotometrically using a modified Cline's method.[40] Sulfate
162 was analyzed by ion chromatography on a Dionex ICS-2100 (Thermo-Fisher, Waltham, MA).
163 Iron and manganese were analyzed by ICP-MS on an Agilent 8900 (Agilent, Santa Clara, CA).
164 DOC was analyzed by a Shimadzu TOC-L using a modified U.S. EPA Method 415.3.[41]

165 *Microbial analyses*

166 Details of microbial analyses are found in SI Sections S1.5-S1.7. DNA was extracted
167 using a modified phenol-chloroform extraction with chemical and physical lysis and purified by
168 ethanol precipitation.[23,42] Samples for RNA extraction were spiked with 12 ng of a 1.3 kbp
169 internal standard transcribed from the pFN18a HaloTag T7 plasmid (Promega, Madison, WI).[43,44]
170 RNA was extracted with Trizol (Thermo-Fisher, Waltham, MA) and precipitated using
171 isopropanol. Sequencing libraries for both DNA and RNA were prepared with a Kapa HyperPrep
172 kit, including ribosomal RNA depletion by RiboErase for the RNA samples (Kapa Biosystems,
173 Wilmington, MA); then, 150 bp paired-end reads were generated using a NovaSeq (Illumina, San
174 Diego, CA). All nucleic acid library preparation and sequencing was completed at the California
175 Institute for Quantitative Biosciences at the University of California-Berkeley. DNA sequences

were quality-trimmed[45] and assembled into contigs,[46] then open reading frames were predicted[47] and sequencing coverage of the contigs was calculated.[48,49] For each metagenome, a genome equivalent value was calculated for 16 single copy core genes[50] by summing the read coverage of each gene; the final genome equivalent for each metagenome was calculated as the median of these values. The relative abundance of each gene of interest in a metagenome was then calculated by normalizing to the number of genome equivalents for that metagenome:

Equation 4: Relative abundance = read coverage of gene / genome equivalents * 100%

Thus, gene abundance is presented as the percentage of the microbial community with that gene. HgcA amino acid sequences were identified using a custom Hidden Markov Model (HMM)[23] and verified to include critical sequence domains.[20,51] Other metabolic genes were identified in the assembly open reading frames using HMMs. All assembly-based gene annotations were manually verified by phylogenetic comparison to reference sequences. Genomic bins were generated using multiple automatic and manual binning strategies[52–56] and subsequently dereplicated using a 96% average nucleotide identity cutoff. Metabolic genes were predicted using convergent methods and manually verified to include important residues. RNA reads were trimmed[45] and residual rRNA reads were removed. Using the internal standard, a normalization factor (NF_{mRNA}) was calculated for each metatranscriptome to convert read counts to mRNA copies per liter as follows:

Equation 5: $NF_{mRNA} = IS_{copies} / (IS_{reads} / IS_{length}) / (\text{Liters of sample filtered})$

where IS_{copies} is the number of internal standard copies added to the extraction, IS_{reads} is the number of pseudo-aligned reads to the internal standard reference, and IS_{length} is the length in base pairs of the internal standard. Remaining mRNA reads were pseudo-aligned[57] to ORFs

predicted from both assemblies and bins. The transcript concentration of each gene of interest (in copies per liter) of was calculated as follows:

Equation 6: Transcript concentration = $GOI_{reads} / GOI_{length} * NF_{mRNA}$

where GOI_{reads} is the number of pseudo-aligned reads to the gene of interest and GOI_{length} is the length in base pairs of the gene of interest. Leucine uptake assays were conducted by incubating water samples at *in situ* conditions with 150 nM tritiated-leucine for 1 hour, analyzed using a scintillation counter, and converted to bacterial carbon production using established methods.[58]

Data availability

Metagenomic and metatranscriptomic data files are available on NCBI (BioProject Accession #PRJNA876614). Files for genomic bins carrying *hgcA* can be found on the Open Science Framework: https://osf.io/9vwgt/. The code used to process and analyze the data is available on GitHub: https://github.com/petersonben50/BLiMMP. Water chemistry and incubations data are available in the corresponding USGS data release.[59]

Results and Discussion

Biogeochemical conditions of Lake Mendota

Samples were collected twice per year during late stratification (once in September, once in October) in both 2020 and 2021 (Fig. 1). Previous work showed that MeHg and *hgcA* abundance is highest during this period.[23] Additionally, this period immediately precedes lake turnover, which is a common driver of MeHg uptake into the food web.[60,61] Eutrophication in Lake Mendota caused elevated primary production and subsequent high biological oxygen

219 demand in the hypolimnion; combined with thermal stratification starting in late May/early June,
220 hypolimnetic oxygen depletion started in July (Fig. S2).[23,62–66] Complete details on
221 biogeochemical measurements are in SI – Section S2.1 (Fig. S3). Previous work has shown little
222 to no detectable nitrate or nitrite in the metalimnion and hypolimnion in Mendota after August
223 due to denitrification.[23,63,67] Elevated particulate manganese (Mn) in the oxycline (maximum at
224 oxycline = 0.101 mg/L, mean = 0.019 mg/L) and filter-passing Mn just below the oxic-anoxic
225 interface (maximum below oxic-anoxic interface = 0.383 mg/L, mean = 0.221 mg/L) in October
226 indicate Mn cycling is constrained to the oxic-anoxic interface (Fig. 1).[23,68] Particulate and filter-
227 passing iron were both much lower in concentration than Mn (Fig. S3), which is likely due to the
228 elevated sulfide levels leading to FeS precipitation.[68] Sulfate levels were over 20 mg/L in the
229 epilimnion. During fall, sulfate reduction led to sulfide levels up to 4.6 mg/L in 2021; however,
230 this is not enough to deplete the sulfate pool, with a minimum measured sulfate concentration of
231 4.7 mg/L (Fig. 1).
232 THg concentrations increased with depth across the anoxic hypolimnion and slightly
233 increased from September to October but exhibited comparable concentrations between both
234 sampling years (i.e., maximum THg in 2020 = 1.37 ng/L, maximum THg in 2021 = 1.41 ng/L;
235 Table S1). Filter-passing MeHg increased with depth across all four sampling dates (Fig. 1).
236 Overall, MeHg concentrations were higher in 2020 (maximum = 0.95 ng/L) than in 2021
237 (maximum = 0.54 ng/L), which was also reflected in the percent MeHg data (2020 maximum =
238 79%, 2021 maximum = 50%). In both years, there was no increase in MeHg concentration or
239 percent MeHg between the September and October sampling events, interpreted to indicate that
240 hypolimnetic MeHg concentrations had reached equilibrium by late stratification. MeHg did not
241 solely account for the increase in THg with depth, as Hg(II) also increased with depth (Fig. 1).

Hg(II) also showed a slight increase from September to October in both years. Conversely to MeHg, Hg(II) was notably lower in 2020 (maximum = 0.7 ng/L) than in 2021 (maximum = 0.91 ng/L). DGM was below 20 pg/L throughout the anoxic hypolimnion in 2021, accounting for a maximum of 2.1% of the THg (mean = 0.7%). This suggests that DGM is not a critical Hg species when evaluating controls on Hg methylation within Lake Mendota.

(De)methylation potentials

The experimental design is shown in Fig. S4 and all Hg speciation data from the incubations are presented in Table S2.[59] Incubation validation metrics are described in SI – Section S2.2 (Figs. S5-S10).

Across the four sets of incubations, the formation of $Me^{198}Hg$ under ambient conditions varied widely based on both date and depth of the incubation. K_{met} ranged from 0.001 day^{-1} to 0.165 day^{-1} (mean = 0.059 ± 0.019 day^{-1}; Fig. 2a). Unless otherwise noted, all mean values are presented as "mean ± standard error of the mean". These K_{met} values are, to our knowledge, the highest reported for water column methylation assays in freshwater (range = 0.01 to 0.06), marine, brackish, and estuarine systems (Table S7).[7–10,22,69–79] This rapid methylation could be due to prime Hg(II) methylation conditions in Lake Mendota, given the supply of labile carbon from the highly productive epilimnion and the elevated sulfate levels.[23] Other studies have been conducted in mesotrophic or oligotrophic systems[10,75] or with settling particles from the epilimnion[8], which are not directly comparable to the eutrophic conditions present in Lake Mendota. Alternatively, the differences could be methodological, as other studies did not pre-equilibrate the enriched Hg isotopes with DOC and/or used glass serum bottles, which could scavenge or sorb the isotopically enriched Hg(II) and thus underestimate K_{met}.[10,75,76] Regardless, these data highlight the rapid formation of MeHg in this dimictic, eutrophic freshwater lake, with

265 up to 50-60% of the ^{198}Hg(II) being methylated within 3.5 days under moderately sulfidic (~2-4
266 mg/L) conditions.

267 Demethylation rates were quantified using Me^{204}Hg. The filtered control incubations
268 showed increasing K_{dem} values with increasing sulfide, leveling off to ~0.2 day^{-1} when sulfide
269 reached ~1.25 mg/L, suggesting possible abiotic demethylation (Fig. S11). These rates are
270 consistent with previously observed K_{dem} values in non-Hg(II)-impacted sites.[38] Interestingly,
271 K_{dem} values in 2021 under ambient conditions were comparable to those from filtered
272 incubations. However, in 2020 there was no demethylation activity under ambient conditions
273 (K_{dem} = ~0 day^{-1}). The higher K_{met} values in 2020 are unlikely to completely negate the proposed
274 abiotic demethylation. These observations suggest a complex control of demethylation rates with
275 multiple demethylation processes occurring simultaneously, with substantial interannual
276 variation. MeHg can be photochemically demethylated by UVA, UVA, or PAR light;[80] however,
277 this is unlikely to be a dominant process due to rapid light attenuation in the highly productive
278 eutrophic waters during the summer and fall months. There are several potential microbial
279 pathways for demethylation. While we identified several homologs of *merB*, one of the best
280 studied biotic demethylation pathways,[81] these homologs did not possess all the requisite
281 conserved amino acid residues[82] and were not contained within a *mer* operon, suggesting they
282 were not true *merB* genes. Methanogens and methanotrophs have also been shown to degrade
283 MeHg through oxidative demethylation.[83–85] However, neither methanotrophs nor methanogens
284 were observed at high abundance in the hypolimnion (data not shown). Dark abiotic
285 demethylation has been documented to reduce up to 5% of the MeHg pool after 10.5 hours,
286 although the mechanism for this is unclear.[80] Regardless, further work is necessary to identify the
287 active demethylation pathways and their drivers in the anoxic hypolimnion.

We compared the K_{met} and K_{dem} values to the ambient MeHg concentrations and percent MeHg levels in the water column. The higher K_{met} values in 2020 (Fig. 2a) corresponded to higher MeHg concentrations and percent MeHg in 2020 than 2021 (Fig. 1). K_{dem} values were higher in 2021, which could also contribute to reduced overall MeHg in the water column. Two lines of evidence suggest that hypolimnetic MeHg concentrations were at equilibrium: first, water column MeHg concentration and percent MeHg showed little change from September to October (Fig. 1); and second, ambient MeHg concentrations in the bags under all treatment conditions remained consistent over the incubation period (Fig. S12; THg data in Fig. S13). If equilibrium has been reached, and assuming the absence of significant external sources or sinks, we can thus assume that K_{met}/K_{dem} = MeHg/Hg(II).[86] To investigate this assumption and test the predictive power of measured K_{met} and K_{dem} values for Hg speciation, we plotted MeHg/Hg(II) against K_{met}/K_{dem} for each incubation location (Fig. S14). Given the uncertainty in the K_{dem} measurements from this study, these values should be interpreted cautiously. However, in general the values were close to the 1:1 line, indicating that the measured rate potentials predict the overall Hg speciation relatively well. This is consistent with *in situ* methylation and demethylation as the primary constraints on MeHg concentrations in the hypolimnion. We hypothesize that deviations from the 1:1 line are due to changes in Hg bioavailability or MeHg sources from other parts of the water column. Samples with a high K_{met}/K_{dem} ratio tended to fall below the 1:1 line, which may indicate a limitation on the bioavailability of the ambient Hg(II) pool. Samples with a low K_{met}/K_{dem} ratio tended to fall above the 1:1 line, possibly indicating an external source of MeHg. The sample with the largest discrepancy in this direction was from near the oxycline in 2021, where MeHg could be enriched by MeHg binding to Mn oxides that form, settle, and redissolve, similar to enrichment in Fe through the "ferrous wheel".[87,88] Overall,

311 these data indicate that MeHg in the water column can be predominantly controlled by *in situ*
312 water column processes of methylation and demethylation.

313 *Biogeochemical drivers of MeHg formation*

314 We then further investigated the biogeochemical constraints on K_{met}. In general, K_{met}
315 increased with increasing sulfide concentrations (Fig. 2a); however, above a threshold
316 concentration of sulfide (~2.4 mg/L in 2020, ~3.8 mg/L in 2021), K_{met} values decreased
317 drastically. This is consistent with the so-called "Goldilocks curve", where MeHg concentrations
318 and/or formation rates exhibit a unimodal distribution along a sulfide gradient due to sulfide's
319 role in both Hg(II) bioavailability and Hg methylation capacity.[22,23,89] The DOC concentration
320 and reduced sulfur content and aromaticity of DOM are three other primary factors governing
321 Hg(II) bioavailability;[14–17] however, DOC concentrations only range from 3.9 to 5.4 mg/L across
322 the different incubation waters (Fig. S3), and previous studies have shown relatively limited
323 variation in DOM aromaticity and reduced sulfur content over the late stratified period in Lake
324 Mendota.[90] We conclude that sulfide is the primary driver of variation in Hg(II) bioavailability
325 across the different incubations, and propose that the decrease in K_{met} values above the sulfide
326 threshold was due to the aggregation of nano-particulate metacinnabar (β-HgS) and subsequent
327 reduction in Hg(II) bioavailability,[16,17] as observed in similar (anoxic and sulfidic) aquatic
328 systems.[21,22]

329 To investigate the role of microbial methylation potential in driving the K_{met} values, we
330 quantified the relative abundance and transcription of 80 unique metagenome-derived *hgcA*
331 genes from a subset of samples along the sulfide gradient (Tables S4, S5, S6). Relative *hgcA*
332 gene abundance ranged from 0.3% to 16.3% of the total microbial community (mean = 7.5 ±
333 1.6%). This range is consistent with previously reported values for sulfidic freshwater lakes[6,9,23],

freshwater peatlands,[13] and marine waters.[91,92] *hgcA* transcript abundance ranged from 1.0 to 7.9 million transcripts per liter (mean = 3.1 ± 0.7 million transcripts per liter); to our knowledge, these are the first measurements of the absolute concentration of *hgcA* gene transcripts in the environment. Gene abundance of *hgcA* increased linearly with increasing sulfide ($p < 0.05$; Fig. S15a), but K_{met} showed a bell-shaped relationship with *hgcA* abundance (Fig. 2B). On the other hand, *hgcA* transcript concentrations peaked at moderate sulfide concentrations (Fig. 15b) and K_{met} increased with increasing *hgcA* transcripts (Fig. 2c); however, this relationship was non-significant ($p = 0.11$), possibly due to the limited sample numbers and no metatranscriptomic data from the low sulfide/low K_{met} locations. Thus, decreased *hgcA* transcription under high sulfide conditions is potentially also responsible for the reduced K_{met} in addition to the abiotic effects of sulfide on Hg speciation. Alternatively, the reduced *hgcA* transcription under sulfidic conditions could be interpreted as a downregulation of the *hgcA* gene in response to reduced Hg(II) bioavailability, which could indicate that the native function of the *hgcA* gene is to methylate and export intracellular Hg(II). However, this is an unlikely explanation given the lack of evidence in the literature for Hg(II)-dependent changes in *hgcA* expression[26,93,94] and the consistent *hgcA* expression across the sulfide gradient within individual microbial populations (see below).

Together, these data suggest a synergistic effect of Hg(II) bioavailability and microbial methylation capacity on MeHg formation, with increasing microbial methylation potential and decreasing Hg(II) bioavailability as sulfide increases leading to the canonical unimodal Goldilocks curve. These hypothesized mechanisms are consistent with the historical understanding of the microbial and biogeochemical factors that underpin Hg methylation[89] and with recent studies in anoxic marine systems[22] and sulfate-enriched freshwater sediments[21]. In a

recent study in a DOM-rich environment, Hg(II) bioavailability was not constrained by sulfide concentration, but rather was dominated by the gradient in DOM concentration and composition (DOM aromaticity and reduced S content).[13] However, similar to this study, Hg(II) methylation was greatest under conditions of *hgcA* abundance and where DOM chemistry promotes Hg(II) bioavailability. These observations highlight the consistent interactions between microbial methylation potential and Hg(II) bioavailability, regardless of the underlying biogeochemical constraints. They also highlight the complexity of the influence of sulfur cycling and DOM chemistry on MeHg production and the need for future investigations of these factors across different environmental systems.

Microbial metabolic drivers of mercury methylation

We also investigated the microbial metabolic processes driving the high Hg(II) methylation capacity in Lake Mendota. Previous studies have implicated SRB,[5,18,95] methanogens,[96,97] iron/manganese-reducers,[98,99] and nitrate-reducing bacteria[6] as likely drivers of MeHg formation in various environments. As we previously observed[23] and as discussed above, both sulfate and sulfide were prevalent throughout the hypolimnion during late stratification, while nitrate and particulate manganese and iron were nearly undetectable (Fig. 1, S3; Table S1). The importance of SRB was further supported by the sequencing data; while respiratory nitrate-reductase (*narG*; associated with nitrate-reducing bacteria) was more abundant than reductive dissimilatory sulfite reductase (*dsrA;* associated with SRB; Fig. S16a), *dsrA* expression was 2-3 orders of magnitude higher than *narG* (Fig. S16b). Methanogen-associated methyl coenzyme M reductase and canonical iron- and manganese-reducing external electron transfer genes were only sporadically detected throughout the hypolimnion and only at low abundance and transcription, indicating those processes are relatively less active, constrained to specific regions of the

hypolimnion, and likely less important for driving microbial metabolism and MeHg formation. Collectively, these data further support sulfate reduction as the dominant terminal electron accepting process in the Lake Mendota hypolimnion during late stratification.[100,101]

To directly measure the influence of SRB on MeHg formation, we calculated a non-SRB-dependent K_{met} ($^{nonSRB}K_{met}$) and an SRB-dependent K_{met} ($^{SRB}K_{met}$) based on the molybdate-amended incubations. $^{nonSRB}K_{met}$ ranged from 0.000 to 0.037 day^{-1} (mean = 0.015 ± 0.005 day^{-1}; Table S3) and were significantly lower than ambient K_{met} (Fig. S17; two-way ANOVA, $p < 0.05$). There was also an interactive effect between sulfide and molybdate amendment ($p < 0.05$), suggesting that the effects of molybdate varied across different redox conditions. $^{SRB}K_{met}$ ranged from 0.003 to 0.129 day^{-1} (mean = 0.054 ± 0.018 day^{-1}). When K_{met} was above 0.002 day^{-1} (at 8 locations), $^{SRB}K_{met}$ accounted for 57.2 to 84.0% of the total K_{met} (mean = 70.3 ± 3.9%). Both $^{SRB}K_{met}$ and $^{nonSRB}K_{met}$ increased with increasing sulfide up to a certain threshold (~2.4 mg/L in 2020, ~3.8 mg/L in 2021), when both decreased, likely due to effects of sulfide inhibition on Hg(II) bioavailability, as previously discussed (Fig. 3a).

One possible explanation of the high $^{SRB}K_{met}$ values could be widespread microbial community inhibition by molybdate, either due to inhibition of other metabolic guilds or a reliance of those other guilds (especially obligate fermenters) on SRB for the consumption of their metabolic products. To investigate this, we performed bacterial production assays under molybdate inhibition. Bacterial production was highest just below the oxic-anoxic interface and substantially lower deeper in the hypolimnion (Fig. S18a-c). Notably, MeHg production did not increase as a function of increased overall microbial production, as has been reported elsewhere.[7,102] Additionally, molybdate amendments did not significantly influence bacterial production rates (two-way ANOVA test with sulfide; $p = 0.010$; Fig. S18d). These observations

403 support that molybdate was inhibiting a specific subset of SRB-dependent metabolic pathways
404 that drive MeHg formation but that do not account for a substantial fraction of heterotrophic
405 bacterial production. This is also consistent with work suggesting complex carbon degradation
406 and fermentation, rather than terminal electron accepting processes and fermentative product
407 consumption, are the rate-limiting steps in complex microbial communities under anoxic
408 conditions.[103]

409 To examine the microbial community underlying the response of K_{met} to molybdate, we
410 assigned each verified *hgcA* sequence to a "metabolic guild" (see SI – Section S1.5 for details;
411 Supplemental Data 1; Table S6, S8). Metabolic guilds included SRB, obligate fermenter
412 (FERM), respiratory but of unknown function (RESP), or unknown (UNK). *Kiritimatiellae*
413 (KIR) were retained separately due to their abundance and ambiguous metabolic capabilities.
414 The abundance of different *hgcA*-carrying microbial guilds did not relate to their transcription
415 levels (Fig. S19). The KIR group included the most abundant hgcA+ microbes across all redox
416 conditions (Fig. 3b), consistent with previous studies,[9,23] accounting for 65.5 ± 2.9% of the
417 overall *hgcA* gene abundance. However, they only accounted for 15.8 ± 3.5% of the *hgcA* mRNA
418 reads (Fig. 3c). RESP *hgcA* sequences were also more abundant in the metagenomes (17.2 ±
419 2.6%) than the metatranscriptomes (8.9 ± 2.5%). The SRB *hgcA* genes were the opposite; they
420 accounted for only 7.5 ± 1.3% of the total *hgcA* gene coverage, but 54.6 ± 4.5% of the *hgcA*
421 mRNA reads. Given that $^{SRB}K_{met}$ accounts for 57.2 to 84.0% of K_{met}, this suggests that gene
422 expression data can predict the biogeochemical drivers of MeHg production better than gene
423 abundance data (Fig. S20). FERM and UNK *hgcA* sequences were low in abundance in both the
424 metagenomes and metatranscriptomes, with the exception that one UNK *hgcA* sequence showed
425 high expression at one location. Both SRB and KIR sequences generally increased with

increasing sulfide concentrations (Fig. 3b,c). We recovered two sets of hgcA+ SRB genomic bins and confirmed that the sulfate reduction pathways were transcriptionally active.

Next, we investigated potential mechanisms underlying differences in *hgcA* expression between metabolic guilds. We used expression of the housekeeping gene *gyrB* and total mRNA levels as a proxy for overall activity of each guild; both were higher among SRB-associated hgcA+ genomic bins compared to FERM- or KIR-associated bins and showed comparable trends to *hgcA* expression (Fig. 4a,b). This suggests that the higher levels of *hgcA* expression in SRBs are due, at least in part, to overall higher levels of transcription rather than specific upregulation of *hgcA*. However, *arsR*-like transcriptional regulators were also identified preceding some of the *hgcA* genes (Fig. 4c). Similar *arsR*-like transcriptional regulators have been identified across multiple environments[19,25,104] and verified to influence *hgcA* expression in the presence of arsenate and arsenite.[26] When *arsR*-like elements were present, other arsenic-cycling genes such as arsenite efflux permeases (*acr3*) or arsenate reductase (*arsC)* were also present in the gene neighborhood (Fig. 4c). While the *arsR*-like elements were not strictly phylogenetically conserved nor exclusively associated with one metabolic guild, they were more commonly found with KIR-associated *hgcA* sequences (Fig. S21). When comparing the 15 most transcriptionally active hgcA+ bins, the presence of the *arsR*-like regulator is associated with significantly lower *hgcA*:*gyrB* transcription ratios (Fig. 4d; two-way ANOVA, $p < 0.05$), suggesting the *arsR*-like element is repressing *hgcA* transcription. However, there was no effect of sulfide concentration ($p = 0.53$) or interaction effect of sulfide and presence of the *arsR*-like element ($p = 0.43$), suggesting that in this system, microbes are not differentially regulating *hgcA* across the redox gradient in response to changing Hg(II) bioavailability or other redox-dependent environmental factor. The *arsR*-like regulators themselves were transcriptionally active, with a transcript

449 concentration slightly higher than the associated *hgcA* sequence (Fig. S22). When taken in
450 context of the recent work by Gionfriddo et al,[26] this highlights the need to further explore the
451 intended function of this *arsR*-like repressor.

452 *Environmental implications*

453 Overall, this study investigates the biogeochemical processes and microbial communities
454 controlling MeHg concentrations in the water column of an urban eutrophic freshwater lake. The
455 high K_{met} values corroborate a growing consensus that water column methylation is an important
456 source of MeHg in freshwater ecosystems, while the demethylation rate potentials indicate
457 complex and possibly competing demethylation processes with substantial year-to-year
458 variability. Together, the paired rate potentials suggest that water column MeHg concentrations
459 in Lake Mendota are driven by *in situ* processes with interannual variation rather than diffusion
460 from sediments or transport from watershed sources, which is consistent with recent
461 literature.[6,8,9,11] This highlights the importance of water quality conditions in determining MeHg
462 accumulation in freshwater ecosystems. While decreasing Hg emissions due to national and
463 international mitigation should result in decreased atmospheric Hg loading to aquatic systems,
464 water quality conditions may negate these reductions and still result in aquatic food web
465 contamination. This study highlights some of these key biogeochemical control points. For
466 example, we bridge a key gap between mesocosm studies showing the importance of SRB in
467 MeHg production and metagenomic studies showing the vast diversity of *hgcA*-carrying
468 microbes and relatively low abundance of *hgcA*-carrying SRB by showing that low abundance,
469 but highly active SRB can drive elevated MeHg production rates. This further reinforces the
470 importance of the sulfur cycle as a key regulator of the Hg cycle and a direct contributor to
471 MeHg formation. However, key questions remain, such as what biogeochemical factors underlie

the distribution and expression of *hgcA*. While this and other studies have shown an increase in *hgcA* with increasing sulfide,[6,22] other work has revealed the opposite trend,[13,21] highlighting the complex controls and site-to-site variation on these processes. Collectively, this highlights the need for mechanistic studies investigating the underlying physiological role of the *hgcAB* gene cluster to enable an ecological perspective on *hgcA* distribution and the Hg methylation phenotype. Studies like the one conducted here are key in illuminating the mechanisms driving MeHg production and will be critical in improving our ability to both effectively manage ecosystems and predict the effects of regional and global change on MeHg formation and Hg accumulation in aquatic food webs.

Figures

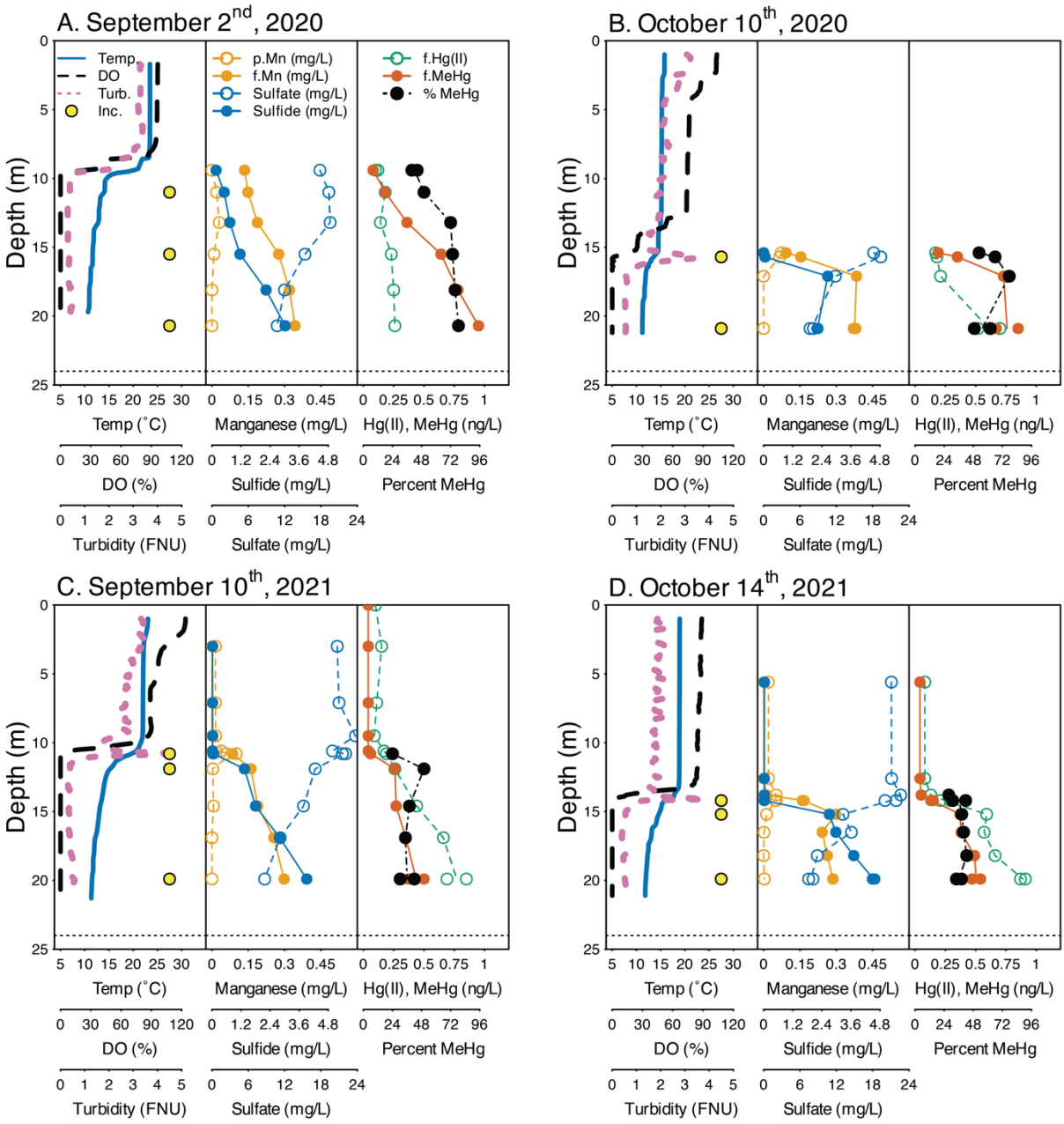

Figure 1: Biogeochemical profiles from Lake Mendota on dates of incubations (A-D). Figure legends are consistent across all four sets of profiles. In B, 15.7 m is indicated as an incubation depth; however, the data is not discussed in the manuscript due to quality control concerns (see text for details). The dotted horizontal lines indicate the sediment-water interface. Temp. =

488 temperature; DO = dissolved oxygen; Turb. = turbidity; Inc. = location of incubation; FNU =
489 Formazin Nephelometric Units; f. = filter-passing; p. = particulate; Mn = manganese; MeHg =
490 methylmercury.
491

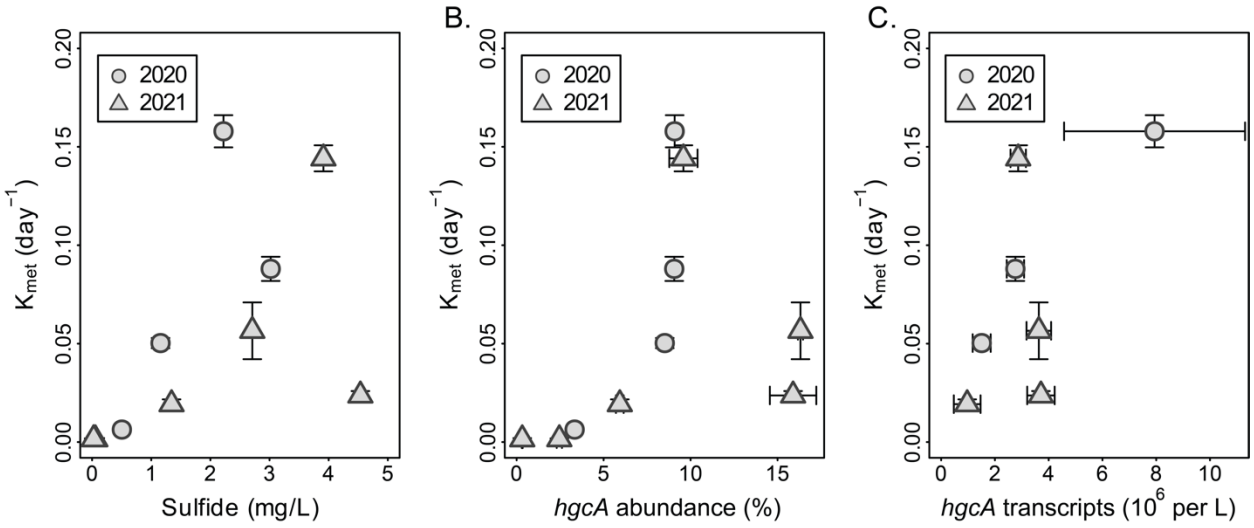

Figure 2: Factors influencing Hg methylation rate potentials in Lake Mendota. K_{met} plotted against sulfide (**A**), relative *hgcA* gene abundance (**B**), and absolute *hgcA* transcript concentrations (**C**). Shapes of the points indicate the year the incubation was conducted. Vertical error bars represent the standard error of the mean (SEM) of K_{met} (**A**-**C**). Horizontal error bars represent the standard deviation of the *hgcA* abundance when duplicate metagenomes were sequenced (**B**) or the SEM of triplicate *hgcA* transcript concentrations (**C**).

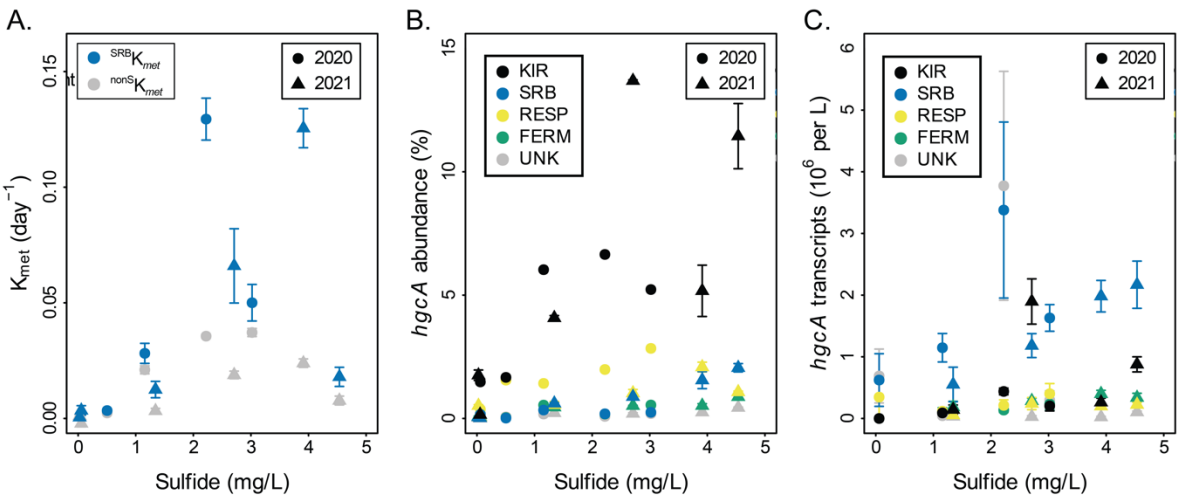

Figure 3: Biogeochemical drivers of methylmercury formation potentials in Lake Mendota. Sulfate-reducing bacteria (SRB)-dependent ($^{SRB}K_{met}$) and -independent K_{met} ($^{nonSRB}K_{met}$) along the sulfide gradient (**A**). Relative abundance (**B**) and absolute transcript concentration (**C**) of *hgcA* from microbial metabolic guilds along the sulfide gradient. Shapes of the points indicate the year the incubation was conducted. Vertical error bars represent the standard error of the mean (SEM) of K_{met} (**A**), the standard deviation of the *hgcA* abundance when duplicate metagenomes were sequenced (**B**), or the SEM of triplicate *hgcA* transcript concentrations (**C**). KIR = *Kiritimatiellaeota*; RESP = respiratory; FERM = obligately fermentative; UNK = unknown metabolic capacity.

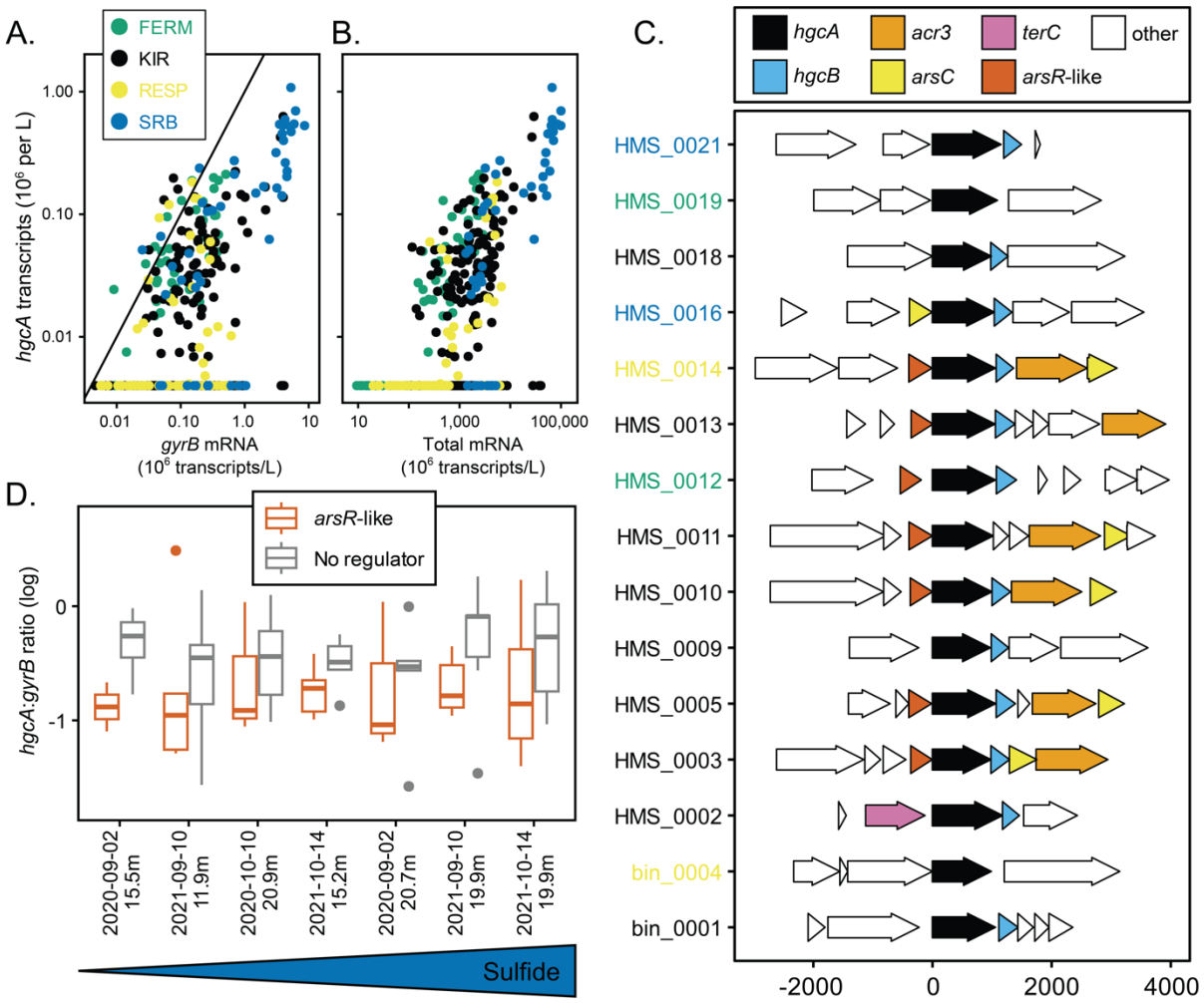

Figure 4: Transcriptional control of *hgcA*. Comparison of *hgcA* transcript concentrations from individual genomic bins in individual metagenomes to *gyrB* transcripts (**A**) or total mRNA (**B**) from the same genomic bin. Gene neighborhood of top 15 most highly expressed *hgcA* genes with homologs of transcriptional regulators and arsenic-related cycling genes color-coded (**C**). Scale on x-axis is base-pair location relative to the start of the *hgcA* gene. Log_{10} ratios of *hgcA* to *gyrB* transcript concentrations for 15 genomic bins with highest expression of *hgcA*, split up by the presence or absence of the *arsR*-like transcriptional regulator (**D**).

Supplementary Materials

Supplementary Tables

Tables include biogeochemical data (Table S1), raw and processed data from assays (Tables S2,S3), sequencing metadata (Table S4), metagenomic statistics (Table S5), *hgcA* gene information (Table S6), literature review of water column mercury methylation studies (Table S7), and bin information for hgcA+ bins (Table S8).

Supplementary Data

Supplemental Data 1 – HgcA tree: HgcA tree RDS object file. This data file contains a ggtree R object of the HgcA amino acids phylogenetic tree that was used to assign taxonomy and metabolic capacity to the *hgcA* sequences.

Acknowledgements

Funding was provided by the USGS Environmental Health Program – Toxics Substances Hydrology program, the USGS-Water Resources Research Institute (WRRI) partnership through coordination grants, and the National Science Foundation grant numbers CBET-1935173 (to K.D.M.) and EAR-2143243 (to B.A.P.). We acknowledge the North Temperate Lakes Long Term Ecological Research (NTL-LTER) site and University of Wisconsin - Madison Center for Limnology for the field and logistical support and for seasonal monitoring data. Computational analyses were performed on the Wisconsin Energy Institute computing cluster, funded by the Great Lakes Bioenergy Research Center through the U.S. Department of Energy Office of Science. Extensive sampling support was provided by Vince Buttita, Tedward Erker, Riley Hale, Marissa Kneer, Angela Magness, Charles Olmsted, Hannah Peterson, Matthew Scarborough, Anna Schmidt, Kathryn Schmidt, and Sarah Stevens. Additional analytical support was provided by John Dewild and Anna Schwendinger. Bag design was supported by Frank Lombardo. Chris Eckley and Jeffra Schaefer provided methodological advice. Any use of trade, product, or firm names in this publication is for descriptive purposes only and does not imply endorsement by the U.S. Government. All authors declare no conflict of interest.

References

(1) U.N. *Global Mercury Assessment*; 2018. https://www.unep.org/resources/publication/global-mercury-assessment-2018.

(2) Wiener, J. G.; Krabbenhoft, D. P.; Heinz, G. H.; Scheuhammer, A. M. Chapter 16: Ecotoxicology of Mercury. In *Handbook of Ecotoxicology*; Hoffman, D. J., Rattner, B. A., Burton, G. A., Cairns, J., Eds.; CRC Press: Boca Raton, Florida, USA, 2003; pp 407–461.

(3) Gilmour, C. C.; Podar, M.; Bullock, A. L.; Graham, A. M.; Brown, S. D.; Somenahally, A. C.; Johs, A.; Hurt, R. A.; Bailey, K. L.; Elias, D. A. Mercury Methylation by Novel Microorganisms from New Environments. *Environ. Sci. Technol.* **2013**, *47* (20), 11810–11820. https://doi.org/10.1021/es403075t.

(4) Hsu-Kim, H.; Kucharzyk, K. H.; Zhang, T.; Deshusses, M. A. Mechanisms Regulating Mercury Bioavailability for Methylating Microorganisms in the Aquatic Environment: A Critical Review. *Environ. Sci. Technol.* **2013**, *47* (6), 2441–2456. https://doi.org/10.1021/es304370g.

(5) Compeau, G. C.; Bartha, R. Sulfate-Reducing Bacteria: Principal Methylators of Mercury in Anoxic Estuarine Sediment. *Appl. Environ. Microbiol.* **1985**, *50* (2), 498–502.

(6) Peterson, B. D.; Poulin, B. A.; Krabbenhoft, D. P.; Tate, M. T.; Baldwin, A. K.; Naymik, J.; Gastelecutto, N.; McMahon, K. D. Metabolically Diverse Microorganisms Mediate Methylmercury Formation under Nitrate-Reducing Conditions in a Dynamic Hydroelectric Reservoir. *ISME J* **2023**, *17*, 1705–1718. https://doi.org/10.1038/s41396-023-01482-1.

(7) Watras, C. J.; Bloom, N. S.; Claas, S. A.; Morrison, K. A.; Gilmour, C. C.; Craig, S. R. Methylmercury Production in the Anoxic Hypolimnion of a Dimictic Seepage Lake. *Water, Air, and Soil Pollution* **1995**, *80*, 735–745. https://doi.org/10.1007/BF01189725.

(8) Gascón Díez, E.; Loizeau, J.-L.; Cosio, C.; Bouchet, S.; Adatte, T.; Amouroux, D.; Bravo, A. G. Role of Settling Particles on Mercury Methylation in the Oxic Water Column of Freshwater Systems. *Environ. Sci. Technol.* **2016**, *50* (21), 11672–11679. https://doi.org/10.1021/acs.est.6b03260.

(9) Jones, D. S.; Walker, G. M.; Johnson, N. W.; Mitchell, C. P. J.; Coleman Wasik, J. K.; Bailey, J. V. Molecular Evidence for Novel Mercury Methylating Microorganisms in Sulfate-Impacted Lakes. *ISME J.* **2019**, *13*, 1659–1675. https://doi.org/10.1038/s41396-019-0376-1.

(10) Eckley, C. S.; Watras, C. J.; Hintelmann, H.; Morrison, K.; Kent, A. D.; Regnell, O. Mercury Methylation in the Hypolimnetic Waters of Lakes with and without Connection to Wetlands in Northern Wisconsin. *Can J Fish Aquat Sci* **2005**, *62* (2), 400–411. https://doi.org/10.1139/f04-205.

(11) Gallorini, A.; Loizeau, J.-L. Lake Snow as a Mercury Methylation Micro-Environment in the Oxic Water Column of a Deep Peri-Alpine Lake. *Chemosphere* **2022**, *299*, 134306. https://doi.org/10.1016/j.chemosphere.2022.134306.

(12) Stoddard, J. L.; Van Sickle, J.; Herlihy, A. T.; Brahney, J.; Paulsen, S.; Peck, D. V.; Mitchell, R.; Pollard, A. I. Continental-Scale Increase in Lake and Stream Phosphorus: Are Oligotrophic Systems Disappearing in the United States? *Environ. Sci. Technol.* **2016**, *50* (7), 3409–3415. https://doi.org/10.1021/acs.est.5b05950.

(13) Peterson, B. D.; Krabbenhoft, D. P.; McMahon, K. D.; Ogorek, J. M.; Tate, M. T.; Orem, W. H.; Poulin, B. A. Environmental Formation of Methylmercury Is Controlled by Synergy of Inorganic Mercury Bioavailability and Microbial Mercury-methylation

Capacity. *Environ. Microbiol.* **2023**, *25* (8), 1409–1423. https://doi.org/10.1111/1462-2920.16364.

(14) Graham, A. M.; Aiken, G. R.; Gilmour, C. C. Effect of Dissolved Organic Matter Source and Character on Microbial Hg Methylation in Hg–S–DOM Solutions. *Environ. Sci. Technol.* **2013**, *47* (11), 5746–5754. https://doi.org/10.1021/es400414a.

(15) Graham, A. M.; Cameron-Burr, K. T.; Hajic, H. A.; Lee, C.; Msekela, D.; Gilmour, C. C. Sulfurization of Dissolved Organic Matter Increases Hg–Sulfide–Dissolved Organic Matter Bioavailability to a Hg-Methylating Bacterium. *Environ. Sci. Technol.* **2017**, *51* (16), 9080–9088. https://doi.org/10.1021/acs.est.7b02781.

(16) Gerbig, C. A.; Kim, C. S.; Stegemeier, J. P.; Ryan, J. N.; Aiken, G. R. Formation of Nanocolloidal Metacinnabar in Mercury-DOM-Sulfide Systems. *Environ. Sci. Technol.* **2011**, *45* (21), 9180–9187. https://doi.org/10.1021/es201837h.

(17) Poulin, B. A.; Gerbig, C. A.; Kim, C. S.; Stegemeier, J. P.; Ryan, J. N.; Aiken, G. R. Effects of Sulfide Concentration and Dissolved Organic Matter Characteristics on the Structure of Nanocolloidal Metacinnabar. *Environ. Sci. Technol.* **2017**, *51* (22), 13133–13142. https://doi.org/10.1021/acs.est.7b02687.

(18) Gilmour, C. C.; Henry, E. A.; Mitchell, R. Sulfate Stimulation of Mercury Methylation in Freshwater Sediments. *Environ. Sci. Technol.* **1992**, *26* (11), 2281–2287. https://doi.org/10.1021/es00035a029.

(19) McDaniel, E. A.; Peterson, B. D.; Stevens, S. L. R.; Tran, P. Q.; Anantharaman, K.; McMahon, K. D. Expanded Phylogenetic Diversity and Metabolic Flexibility of Mercury-Methylating Microorganisms. *mSystems* **2020**, *5* (4), e00299-20. https://doi.org/10.1128/mSystems.00299-20.

(20) Parks, J. M.; Johs, A.; Podar, M.; Bridou, R.; Hurt, R. A.; Smith, S. D.; Tomanicek, S. J.; Qian, Y.; Brown, S. D.; Brandt, C. C.; Palumbo, A. V.; Smith, J. C.; Wall, J. D.; Elias, D. A.; Liang, L. The Genetic Basis for Bacterial Mercury Methylation. *Science* **2013**, *339* (6125), 1332–1335. https://doi.org/10.1126/science.1230667.

(21) Jones, D. S.; Johnson, N. W.; Mitchell, C. P. J.; Walker, G. M.; Bailey, J. V.; Pastor, J.; Swain, E. B. Diverse Communities of *hgcAB*$^{+}$ Microorganisms Methylate Mercury in Freshwater Sediments Subjected to Experimental Sulfate Loading. *Environ. Sci. Technol.* **2020**, *54*, 14265−14274. https://doi.org/10.1021/acs.est.0c02513.

(22) Capo, E.; Feng, C.; Bravo, A. G.; Bertilsson, S.; Soerensen, A. L.; Pinhassi, J.; Buck, M.; Karlsson, C.; Hawkes, J.; Björn, E. Expression Levels of *hgcAB* Genes and Mercury Availability Jointly Explain Methylmercury Formation in Stratified Brackish Waters. *Environ. Sci. Technol.* **2022**, *56* (18), 13119–13130. https://doi.org/10.1021/acs.est.2c03784.

(23) Peterson, B. D.; McDaniel, E. A.; Schmidt, A. G.; Lepak, R. F.; Janssen, S. E.; Tran, P. Q.; Marick, R. A.; Ogorek, J. M.; DeWild, J. F.; Krabbenhoft, D. P.; McMahon, K. D. Mercury Methylation Genes Identified across Diverse Anaerobic Microbial Guilds in a Eutrophic Sulfate-Enriched Lake. *Environ. Sci. Technol.* **2020**, *54*, 15840–15851. https://doi.org/10.1021/acs.est.0c05435.

(24) Bae, H.-S.; Dierberg, F. E.; Ogram, A. Syntrophs Dominate Sequences Associated with the Mercury Methylation-Related Gene *hgcA* in the Water Conservation Areas of the Florida Everglades. *Appl. Environ. Microbiol.* **2014**, *80* (20), 6517–6526. https://doi.org/10.1128/AEM.01666-14.

(25) Goñi-Urriza, M.; Klopp, C.; Ranchou-Peyruse, M.; Ranchou-Peyruse, A.; Monperrus, M.; Khalfaoui-Hassani, B.; Guyoneaud, R. Genome Insights of Mercury Methylation among *Desulfovibrio* and *Pseudodesulfovibrio* Strains. *Research in Microbiology* **2020**, *171* (1), 3–12. https://doi.org/10.1016/j.resmic.2019.10.003.

(26) Gionfriddo, C. M.; Soren, A. B.; Wymore, A. M.; Hartnett, D. S.; Podar, M.; Parks, J. M.; Elias, D. A.; Gilmour, C. C. Transcriptional Control of *hgcAB* by an ArsR-Like Regulator in *Pseudodesulfovibrio Mercurii* ND132. *Appl. Environ. Microbiol.* **2023**, *89* (4), e01768-22. https://doi.org/10.1128/aem.01768-22.

(27) Olson, M. L.; DeWild, J. F. Techniques for the Collection and Species-Specific Analysis of Low Levels of Mercury in Water, Sediment, and Biota. In *U.S. Geological Survey Water-Resources Investigations Report*; Washington, D.C., 1999; Vol. 99-4018B.

(28) Poulain, A. J.; Amyot, M.; Findlay, D.; Telor, S.; Barkay, T.; Hintelmann, H. Biological and Photochemical Production of Dissolved Gaseous Mercury in a Boreal Lake. *Limnology & Oceanography* **2004**, *49* (6), 2265–2275. https://doi.org/10.4319/lo.2004.49.6.2265.

(29) Gilmour, C. C.; Riedel, G. S.; Ederington, M. C.; Bell, J. T.; Benoit, J. M.; Gill, G. A.; Stordal, M. C. Methylmercury Concentrations and Production Rates across a Trophic Gradient in the Northern Everglades. *Biogeochemistry* **1998**, *40*, 327–345. https://doi.org/10.1023/A:1005972708616.

(30) Oremland, R. S.; Capone, D. G. Use of "Specific" Inhibitors in Biogeochemistry and Microbial Ecology. In *Advances in Microbial Ecology*; Marshall, K. C., Ed.; Springer US: Boston, MA, 1988; pp 285–383. https://doi.org/10.1007/978-1-4684-5409-3_8.

(31) U.S. EPA. *U.S. EPA Method 1631, Revision E: Mercury in Water by Oxidation, Purge and Trap, And Cold Vapor Atomic Fluorescence Spectrometry*; U.S. Environmental Protection Agency: Washington, D.C., 2002.

(32) DeWild, J. F.; Olson, M. L.; Olund, S. D. *Determination of Methyl Mercury by Aqueous Phase Ethylation, Followed by Gas Chromatographic Separation with Cold Vapor Atomic Fluorescence Detection. Open-File Report*; Open-File Report; 01–445; U. S. Geological Survey: Reston, VA, 2002.

(33) Horvat, M.; Bloom, N. S.; Liang, L. Comparison of Distillation with Other Current Isolation Methods for the Determination of Methyl Mercury Compounds in Low Level Environmental Samples. *Analytica Chimica Acta* **1993**, *281*, 135–152. https://doi.org/10.1016/0003-2670(93)85348-N.

(34) Lepak, R. F.; Krabbenhoft, D. P.; Ogorek, J. M.; Tate, M. T.; Bootsma, H. A.; Hurley, J. P. Influence of *Cladophora*–Quagga Mussel Assemblages on Nearshore Methylmercury Production in Lake Michigan. *Environ. Sci. Technol.* **2015**, *49* (13), 7606–7613. https://doi.org/10.1021/es506253v.

(35) Hintelmann, H.; Evans, R. D. Application of Stable Isotopes in Environmental Tracer Studies - Measurement of Monomethylmercury (CH_3Hg^+) by Isotope Dilution ICP-MS and Detection of Species Transformation. *Fresenius J. Anal. Chem.* **1997**, *358* (3), 378–385. https://doi.org/10.1007/s002160050433.

(36) Hintelmann, H.; Evans, R. D.; Villeneuve, J. Y. Measurement of Mercury Methylation in Sediments by Using Enriched Stable Mercury Isotopes Combined with Methylmercury Determination by Gas Chromatography–Inductively Coupled Plasma Mass Spectrometry. *J. Anal. At. Spectrom.* **1995**, *10* (9), 619–624. https://doi.org/10.1039/JA9951000619.

(37) Marvin-DiPasquale, M.; Agee, J. L. Microbial Mercury Cycling in Sediments of the San Francisco Bay-Delta. *Estuaries* **2003**, *26* (6), 1517–1528. https://doi.org/10.1007/BF02803660.
(38) Helmrich, S.; Vlassopoulos, D.; Alpers, C. N.; O'Day, P. A. Critical Review of Mercury Methylation and Methylmercury Demethylation Rate Constants in Aquatic Sediments for Biogeochemical Modeling. *Crit. Rev. Environ. Sci. Technol.* **2022**, *52* (24), 4353–4378. https://doi.org/10.1080/10643389.2021.2013073.
(39) Ramlal, P. S.; Rudd, J. W. M.; Hecky, R. E. Methods for Measuring Specific Rates of Mercury Methylation and Degradation and Their Use in Determining Factors Controlling Net Rates of Mercury Methylation. *Appl. Environ. Microbiol.* **1986**, *51* (1), 110–114. https://doi.org/10.1128/aem.51.1.110-114.1986.
(40) Cline, J. D. Spectrophotometric Determination of Hydrogen Sulfide in Natural Waters. *Limnol. Oceanogr.* **1969**, *14* (3), 454–458. https://doi.org/10.4319/lo.1969.14.3.0454.
(41) Potter, B. B.; Wimsatt, J. C. USEPA Method 415.3: Quantifying TOC, DOC, and SUVA. *Journal AWWA* **2012**, *104* (6), E358–E369. https://doi.org/10.5942/jawwa.2012.104.0086.
(42) Lever, M. A.; Torti, A.; Eickenbusch, P.; Michaud, A. B.; Šantl-Temkiv, T.; Jørgensen, B. B. A Modular Method for the Extraction of DNA and RNA, and the Separation of DNA Pools from Diverse Environmental Sample Types. *Front. Microbiol.* **2015**, *6*, 476. https://doi.org/10.3389/fmicb.2015.00476.
(43) Satinsky, B. M.; Gifford, S. M.; Crump, B. C.; Moran, M. A. Use of Internal Standards for Quantitative Metatranscriptome and Metagenome Analysis. In *Methods in Enzymology*; Elsevier, 2013; Vol. 531, pp 237–250. https://doi.org/10.1016/B978-0-12-407863-5.00012-5.
(44) Linz, A. M.; Aylward, F. O.; Bertilsson, S.; McMahon, K. D. Time-series Metatranscriptomes Reveal Conserved Patterns between Phototrophic and Heterotrophic Microbes in Diverse Freshwater Systems. *Limnol. Oceanogr.* **2020**, *65*, S101–S112. https://doi.org/10.1002/lno.11306.
(45) Chen, S.; Zhou, Y.; Chen, Y.; Gu, J. Fastp: An Ultra-Fast All-in-One FASTQ Preprocessor. *Bioinformatics* **2018**, *34* (17), i884–i890. https://doi.org/10.1093/bioinformatics/bty560.
(46) Nurk, S.; Meleshko, D.; Korobeynikov, A.; Pevzner, P. A. metaSPAdes: A New Versatile Metagenomic Assembler. *Genome Research* **2017**, *27* (5), 824–834. https://doi.org/10.1101/gr.213959.116.
(47) Hyatt, D.; Chen, G.-L.; LoCascio, P. F.; Land, M. L.; Larimer, F. W.; Hauser, L. J. Prodigal: Prokaryotic Gene Recognition and Translation Initiation Site Identification. *BMC Bioinformatics* **2010**, *11*, 119. https://doi.org/10.1186/1471-2105-11-119.
(48) Langmead, B.; Salzberg, S. L. Fast Gapped-Read Alignment with Bowtie 2. *Nat. Methods.* **2012**, *9* (4), 357–359. https://doi.org/10.1038/nmeth.1923.
(49) Li, H.; Handsaker, B.; Wysoker, A.; Fennell, T.; Ruan, J.; Homer, N.; Marth, G.; Abecasis, G.; Durbin, R.; 1000 Genome Project Data Processing Subgroup. The Sequence Alignment/Map Format and SAMtools. *Bioinformatics* **2009**, *25* (16), 2078–2079. https://doi.org/10.1093/bioinformatics/btp352.
(50) Sorek, R.; Zhu, Y.; Creevey, C. J.; Francino, M. P.; Bork, P.; Rubin, E. M. Genome-Wide Experimental Determination of Barriers to Horizontal Gene Transfer. *Science* **2007**, *318* (5855), 1449–1452. https://doi.org/10.1126/science.1147112.

(51) Gionfriddo, C. M.; Capo, E.; Peterson, B. D.; Heyu, L.; Jones, D. S.; Bravo, A. G.; Bertilsson, S.; Moreau, J. W.; McMahon, K. D.; Elias, D. A.; Gilmour, C. C. Hg-MATE-Db.v1.01142021, 2021. https://doi.org/10.25573/serc.13105370.v1.
(52) Kang, D. D.; Li, F.; Kirton, E.; Thomas, A.; Egan, R.; An, H.; Wang, Z. MetaBAT 2: An Adaptive Binning Algorithm for Robust and Efficient Genome Reconstruction from Metagenome Assemblies. *PeerJ* **2019**, *7*, e7359. https://doi.org/10.7717/peerj.7359.
(53) Wu, Y.-W.; Simmons, B. A.; Singer, S. W. MaxBin 2.0: An Automated Binning Algorithm to Recover Genomes from Multiple Metagenomic Datasets. *Bioinformatics* **2016**, *32* (4), 605–607. https://doi.org/10.1093/bioinformatics/btv638.
(54) Sieber, C. M. K.; Probst, A. J.; Sharrar, A.; Thomas, B. C.; Hess, M.; Tringe, S. G.; Banfield, J. F. Recovery of Genomes from Metagenomes via a Dereplication, Aggregation and Scoring Strategy. *Nat Microbiol* **2018**, *3* (7), 836–843. https://doi.org/10.1038/s41564-018-0171-1.
(55) Eren, A. M.; Esen, Ö. C.; Quince, C.; Vineis, J. H.; Morrison, H. G.; Sogin, M. L.; Delmont, T. O. Anvi'o: An Advanced Analysis and Visualization Platform for 'omics Data. *PeerJ* **2015**, *3*, e1319. https://doi.org/10.7717/peerj.1319.
(56) Alneberg, J.; Bjarnason, B. S.; de Bruijn, I.; Schirmer, M.; Quick, J.; Ijaz, U. Z.; Lahti, L.; Loman, N. J.; Andersson, A. F.; Quince, C. Binning Metagenomic Contigs by Coverage and Composition. *Nat. Methods.* **2014**, *11* (11), 1144–1146. https://doi.org/10.1038/nmeth.3103.
(57) Bray, N. L.; Pimentel, H.; Melsted, P.; Pachter, L. Near-Optimal Probabilistic RNA-Seq Quantification. *Nat Biotechnol* **2016**, *34* (5), 525–527. https://doi.org/10.1038/nbt.3519.
(58) Simon, M.; Azam, F. Protein Content and Protein Synthesis Rates of Planktonic Marine Bacteria. *Mar. Ecol. Prog. Ser.* **1989**, *51*, 201–213. https://doi.org/10.3354/meps051201.
(59) Peterson, B. D.; Janssen, S. E.; Tate, M. T.; Poulin, B. A.; McMahon, K. D. *Assessment of Mercury Concentrations and Methylation Rate Potentials in Lake Mendota, Wisconsin, USA*; U.S. Geological Survey Data Release; 2024. https://doi.org/10.5066/P14TO3BL. (accessed 2024-11-11).
(60) Herrin, R. T.; Lathrop, R. C.; Gorski, P. R.; Andren, A. W. Hypolimnetic Methylmercury and Its Uptake by Plankton during Fall Destratification:A Key Entry Point of Mercury into Lake Food Chains? *Limnol. Oceanogr.* **1998**, *43* (7), 1476–1486. https://doi.org/10.4319/lo.1998.43.7.1476.
(61) Slotton, D. G.; Reuter, J. E.; Goldman, C. R. Mercury Uptake Patterns of Biota in a Seasonally Anoxic Northern California Reservoir. *Water, Air, and Soil Pollution* **1995**, *80*, 841–850. https://doi.org/10.1007/BF01189735.
(62) Snortheim, C. A.; Hanson, P. C.; McMahon, K. D.; Read, J. S.; Carey, C. C.; Dugan, H. A. Meteorological Drivers of Hypolimnetic Anoxia in a Eutrophic, North Temperate Lake. *Ecological Modelling* **2017**, *343*, 39–53. https://doi.org/10.1016/j.ecolmodel.2016.10.014.
(63) Brock, T. D. *A Eutrophic Lake: Lake Mendota, Wisconsin*, 1st ed.; Springer, 1985.
(64) Magnuson, J. J.; Carpenter, S. R.; Stanley, E. H. Lake Mendota Multiparameter Sonde Profiles: 2017 - Present, 2023. https://doi.org/10.6073/pasta/361b52d76ed0b9a7f706aec0ca01909b.
(65) Magnuson, J. J.; Carpenter, S. R.; Stanley, E. H. North Temperate Lakes LTER: High Frequency Water Temperature Data - Lake Mendota Buoy 2006 - Current, 2024. https://doi.org/10.6073/pasta/b6b6b2f2070500202e10e219044b547b.

(66) Magnuson, J. J.; Carpenter, S. R.; Stanley, E. H. North Temperate Lakes LTER: High Frequency Data: Meteorological, Dissolved Oxygen, Chlorophyll, Phycocyanin - Lake Mendota Buoy 2006 - Current, 2024. https://doi.org/10.6073/pasta/daad81be7f12173e3aefbf3df5d6d2fe.
(67) Magnuson, J. J.; Carpenter, S. R.; Stanley, E. H. North Temperate Lakes LTER: Chemical Limnology of Primary Study Lakes: Nutrients, pH and Carbon 1981 - Current, 2023. https://doi.org/10.6073/pasta/325232e6e4cd1ce04025fa5674f7b782.
(68) Stauffer, R. E. Cycling of Manganese and Iron in Lake Mendota, Wisconsin. *Environ. Sci. Technol.* **1986**, *20* (5), 449–457. https://doi.org/10.1021/es00147a002.
(69) Schartup, A. T.; Balcom, P. H.; Soerensen, A. L.; Gosnell, K. J.; Calder, R. S. D.; Mason, R. P.; Sunderland, E. M. Freshwater Discharges Drive High Levels of Methylmercury in Arctic Marine Biota. *Proc. Natl. Acad. Sci. U.S.A.* **2015**, *112* (38), 11789–11794. https://doi.org/10.1073/pnas.1505541112.
(70) Soerensen, A. L.; Schartup, A. T.; Skrobonja, A.; Bouchet, S.; Amouroux, D.; Liem-Nguyen, V.; Björn, E. Deciphering the Role of Water Column Redoxclines on Methylmercury Cycling Using Speciation Modeling and Observations from the Baltic Sea. *Global Biogeochem. Cycles* **2018**, *32* (10), 1498–1513. https://doi.org/10.1029/2018GB005942.
(71) Lehnherr, I.; St. Louis, V. L.; Hintelmann, H.; Kirk, J. L. Methylation of Inorganic Mercury in Polar Marine Waters. *Nature Geosci* **2011**, *4* (5), 298–302. https://doi.org/10.1038/ngeo1134.
(72) Malcolm, E. G.; Schaefer, J. K.; Ekstrom, E. B.; Tuit, C. B.; Jayakumar, A.; Park, H.; Ward, B. B.; Morel, F. M. M. Mercury Methylation in Oxygen Deficient Zones of the Oceans: No Evidence for the Predominance of Anaerobes. *Marine Chemistry* **2010**, *122* (1–4), 11–19. https://doi.org/10.1016/j.marchem.2010.08.004.
(73) Monperrus, M.; Tessier, E.; Amouroux, D.; Leynaert, A.; Huonnic, P.; Donard, O. F. X. Mercury Methylation, Demethylation and Reduction Rates in Coastal and Marine Surface Waters of the Mediterranean Sea. *Marine Chemistry* **2007**, *107* (1), 49–63. https://doi.org/10.1016/j.marchem.2007.01.018.
(74) Monperrus, M.; Tessier, E.; Point, D.; Vidimova, K.; Amouroux, D.; Guyoneaud, R.; Leynaert, A.; Grall, J.; Chauvaud, L.; Thouzeau, G.; Donard, O. F. X. The Biogeochemistry of Mercury at the Sediment–Water Interface in the Thau Lagoon. 2. Evaluation of Mercury Methylation Potential in Both Surface Sediment and the Water Column. *Estuarine, Coastal and Shelf Science* **2007**, *72* (3), 485–496. https://doi.org/10.1016/j.ecss.2006.11.014.
(75) Eckley, C. S.; Hintelmann, H. Determination of Mercury Methylation Potentials in the Water Column of Lakes across Canada. *STOTEN* **2006**, *368* (1), 111–125. https://doi.org/10.1016/j.scitotenv.2005.09.042.
(76) Eckley, C. S.; Luxton, T. P.; Knightes, C. D.; Shah, V. Methylmercury Production and Degradation under Light and Dark Conditions in the Water Column of the Hells Canyon Reservoirs, USA. *Enviro. Toxic. and Chemistry* **2021**, *40* (7), 1827–1837. https://doi.org/10.1002/etc.5041.
(77) Matilainen, T. Involvement of Bacteria in Methylmercury Formation in Anaerobic Lake Waters. *Water, Air, and Soil Pollution* **1995**, *80*, 757–764.

(78) Verta, M.; Matilainen, T. Methylmercury Distribution and Partitioning in Stratified Finnish Forest Lakes. *Water, Air, and Soil Pollution* **1995**, *80*, 585–588. https://doi.org/10.1007/978-94-011-0153-0_64.
(79) Korthals, E. T.; Winfrey, M. R. Seasonal and Spatial Variations in Mercury Methylation and Demethylation in an Oligotrophic Lake. *Appl. Environ. Microbiol.* **1987**, *53* (10), 2397–2404. https://doi.org/10.1128/aem.53.10.2397-2404.1987.
(80) Black, F. J.; Poulin, B. A.; Flegal, A. R. Factors Controlling the Abiotic Photo-Degradation of Monomethylmercury in Surface Waters. *Geochimica et Cosmochimica Acta* **2012**, *84*, 492–507. https://doi.org/10.1016/j.gca.2012.01.019.
(81) Barkay, T.; Gu, B. Demethylation - the Other Side of the Mercury Methylation Coin: A Critical Review. *ACS Environ. Au* **2021**, acsenvironau.1c00022. https://doi.org/10.1021/acsenvironau.1c00022.
(82) Christakis, C. A.; Barkay, T.; Boyd, E. S. Expanded Diversity and Phylogeny of *Mer* Genes Broadens Mercury Resistance Paradigms and Reveals an Origin for MerA among Thermophilic Archaea. *Front. Microbiol.* **2021**, *12*. https://doi.org/10.3389/fmicb.2021.682605.
(83) Lu, X.; Gu, W.; Zhao, L.; Haque, M. F. U.; DiSpirito, A. A.; Semrau, J. D.; Gu, B. Methylmercury Uptake and Degradation by Methanotrophs. *Sci. Adv.* **2017**, *3*, e1700041. https://doi.org/10.1126/sciadv.1700041.
(84) Kronberg, R.-M.; Schaefer, J. K.; Björn, E.; Skyllberg, U. Mechanisms of Methyl Mercury Net Degradation in Alder Swamps: The Role of Methanogens and Abiotic Processes. *Environ. Sci. Technol. Lett.* **2018**, *5*, 220–225. https://doi.org/10.1021/acs.estlett.8b00081.
(85) Grégoire, D. S.; Poulain, A. J. Shining Light on Recent Advances in Microbial Mercury Cycling. *FACETS* **2018**, *3* (1), 858–879. https://doi.org/10.1139/facets-2018-0015.
(86) Tjerngren, I.; Meili, M.; Björn, E.; Skyllberg, U. Eight Boreal Wetlands as Sources and Sinks for Methyl Mercury in Relation to Soil Acidity, C/N Ratio, and Small-Scale Flooding. *Environ. Sci. Technol.* **2012**, *46* (15), 8052–8060. https://doi.org/10.1021/es300845x.
(87) Chadwick, S. P.; Babiarz, C. L.; Hurley, J. P.; Armstrong, D. E. Importance of Hypolimnetic Cycling in Aging of "New" Mercury in a Northern Temperate Lake. *Science of The Total Environment* **2013**, *448*, 176–188. https://doi.org/10.1016/j.scitotenv.2012.10.069.
(88) Chadwick, S. P.; Babiarz, C. L.; Hurley, J. P.; Armstrong, D. E. Influences of Iron, Manganese, and Dissolved Organic Carbon on the Hypolimnetic Cycling of Amended Mercury. *STOTEN* **2006**, *368* (1), 177–188. https://doi.org/10.1016/j.scitotenv.2005.09.039.
(89) Gilmour, C. C.; Krabbenhoft, D.; Orem, W. H.; Aiken, G.; Roden, E. *Appendix 3B-2: Status Report on ACME Studies on the Control of Mercury Methylation and Bioaccumulation in the Everglades*; South Florida Environmental Report; Volume 1; South Florida Water Management District, 2007.
(90) Berg, S. M.; Peterson, B. D.; McMahon, K. D.; Remucal, C. K. Spatial and Temporal Variability of Dissolved Organic Matter Molecular Composition in a Stratified Eutrophic Lake. *JGR Biogeosciences* **2022**, *127*, e2021JG006550. https://doi.org/10.1029/2021JG006550.
(91) Lin, H.; Ascher, D. B.; Myung, Y.; Lamborg, C. H.; Hallam, S. J.; Gionfriddo, C. M.; Holt, K. E.; Moreau, J. W. Mercury Methylation by Metabolically Versatile and Cosmopolitan

Marine Bacteria. *ISME J.* **2021**, *15*, 1810–1825. https://doi.org/10.1038/s41396-020-00889-4.

(92) Capo, E.; Cosio, C.; Díez, E. G.; Loizeau, J.-L.; Mendes, E.; Adatte, T.; Franzenburg, S.; Bravo, A. G. Anaerobic Mercury Methylators Inhabit Sinking Particles of Oxic Water Columns. *Water Research* **2023**, *229*, 119368. https://doi.org/10.1016/j.watres.2022.119368.

(93) Gilmour, C. C.; Elias, D. A.; Kucken, A. M.; Brown, S. D.; Palumbo, A. V.; Schadt, C. W.; Wall, J. D. Sulfate-Reducing Bacterium *Desulfovibrio Desulfuricans* ND132 as a Model for Understanding Bacterial Mercury Methylation. *Appl. Environ. Microbiol.* **2011**, *77* (12), 3938–3951. https://doi.org/10.1128/AEM.02993-10.

(94) Qian, C.; Chen, H.; Johs, A.; Lu, X.; An, J.; Pierce, E. M.; Parks, J. M.; Elias, D. A.; Hettich, R. L.; Gu, B. Quantitative Proteomic Analysis of Biological Processes and Responses of the Bacterium *Desulfovibrio Desulfuricans* ND132 upon Deletion of Its Mercury Methylation Genes. *Proteomics* **2018**, *18* (17), 1700479. https://doi.org/10.1002/pmic.201700479.

(95) King, J. K.; Kostka, J. E.; Frischer, M. E.; Saunders, F. M. Sulfate-Reducing Bacteria Methylate Mercury at Variable Rates in Pure Culture and in Marine Sediments. *Appl. Environ. Microbiol.* **2000**, *66* (6), 2430–2437. https://doi.org/10.1128/AEM.66.6.2430-2437.2000.

(96) Kerin, E. J.; Gilmour, C. C.; Roden, E.; Suzuki, M. T.; Coates, J. D.; Mason, R. P. Mercury Methylation by Dissimilatory Iron-Reducing Bacteria. *Appl. Environ. Microbiol.* **2006**, *72* (12), 7919–7921. https://doi.org/10.1128/AEM.01602-06.

(97) Fleming, E. J.; Mack, E. E.; Green, P. G.; Nelson, D. C. Mercury Methylation from Unexpected Sources: Molybdate-Inhibited Freshwater Sediments and an Iron-Reducing Bacterium. *Appl. Environ. Microbiol.* **2006**, *72* (1), 457–464. https://doi.org/10.1128/AEM.72.1.457-464.2006.

(98) Hamelin, S.; Amyot, M.; Barkay, T.; Wang, Y.; Planas, D. Methanogens: Principal Methylators of Mercury in Lake Periphyton. *Environ. Sci. Technol.* **2011**, *45* (18), 7693–7700. https://doi.org/10.1021/es2010072.

(99) Gilmour, C. C.; Bullock, A. L.; McBurney, A.; Podar, M.; Elias, D. A. Robust Mercury Methylation across Diverse Methanogenic *Archaea*. *mBio* **2018**, *9* (2), e02403-17. https://doi.org/10.1128/mBio.02403-17.

(100) Ingvorsen, K.; Brock, T. D. Electron Flow via Sulfate Reduction and Methanogenesis in the Anaerobic Hypolimnion of Lake Mendota. *Limnol. Oceanogr.* **1982**, *27* (3), 559–564. https://doi.org/10.4319/lo.1982.27.3.0559.

(101) Ingvorsen, K.; Zeikus, J. G.; Brock, T. D. Dynamics of Bacterial Sulfate Reduction in a Eutrophic Lake. *Appl. Environ. Microbiol.* **1981**, *42* (6), 1029–1036. https://doi.org/10.1128/AEM.42.6.1029-1036.1981.

(102) Guimarães, J. R. D.; Mauro, J. B. N.; Meili, M.; Sundbom, M.; Haglund, A. L.; Coelho-Souza, S. A.; Hylander, L. D. Simultaneous Radioassays of Bacterial Production and Mercury Methylation in the Periphyton of a Tropical and a Temperate Wetland. *Journal of Environmental Management* **2006**, *81* (2), 95–100. https://doi.org/10.1016/j.jenvman.2005.09.023.

(103) Beulig, F.; Røy, H.; Glombitza, C.; Jørgensen, B. B. Control on Rate and Pathway of Anaerobic Organic Carbon Degradation in the Seabed. *Proc Natl Acad Sci USA* **2018**, *115* (2), 367–372. https://doi.org/10.1073/pnas.1715789115.

(104) Gionfriddo, C. M.; Stott, M. B.; Power, J. F.; Ogorek, J. M.; Krabbenhoft, D. P.; Wick, R.; Holt, K.; Chen, L.-X.; Thomas, B. C.; Banfield, J. F.; Moreau, J. W. Genome-Resolved Metagenomics and Detailed Geochemical Speciation Analyses Yield New Insights into Microbial Mercury Cycling in Geothermal Springs. *Appl. Environ. Microbiol.* **2020**, *86* (15), e00176-20. https://doi.org/10.1128/AEM.00176-20.